Numerical simulation and modeling of the heat and mass transfer in a grooved flat falling film evaporator

R. Collignon, B. Stutz

Numerical simulation and modeling of the heat and mass transfer in a grooved flat falling film evaporator

R. Collignon[1*] and B. Stutz[1]

[1] *Université Savoie Mont Blanc, CNRS, LOCIE, 73000 Chambéry, France*
[*] *Corresponding author*

Abstract

Falling film plate exchanger are used in a wide range of systems thanks to their high heat and mass transfer performance for a low cost. In this study, a grooved plate is considered for it's ability to improve the wetting of the surface compared to a smooth plate. To characterize the heat transfer and evaporation rate of the system, a numerical model has been developed to take account of the new geometry and has been confronted to experimental results. Despite the high aspect ratio of the falling film, the fin effect is very high on the heat transfer and on the vaporization process due to the triple contact lines. The principal aim of this study is to develop a simple and light model able to accurately describe the heat and mass transfer behaviour of film while it flows down in the grooves of the vertical plate of the evaporator. The influence of the operating conditions on the evaporator effectiveness are evaluated thanks to numerical investigations.

Nomenclature

Physical properties

λ	Thermal conductivity [W/m/K]
ν	Kinematic viscosity [m^2/s]
ρ	Volumetric mass density [kg/m^3]
g	Gravitational acceleration [$kg/m/s^2$]
h	Enthalpy [J/kg]
h_{evap}	Latent heat of evaporation [J/kg]
M	Molar mass [kg/mol]
R	Ideal gas constant [J/kg/mol]
H	Thickness of the heat exchanger plate [m]
L	Length of the heat exchanger plate [m]
l	Width of a falling film channel [m]
L_{th}	Establishment length of the thermal boundary layer [m]
P	Pressure [Pa]
q	Heat flux [W]
R_{tl}	Heat transfer resistance [$K \cdot m^2/W$]
T	Temperature [K]

Variables

α	Heat transfer coefficient [$W/m^2/K$]
δ	Thickness of the film [m]
$\dot{m}$	Mass flow rate [kg/s]
$\dot{q}$	Heat flux density [W/m^2]
ϵ	Efficiency
Γ	volumetric flow rate per unit of width [m^2/s]
Pr	Prandtl number
Re	Reynolds number
d_w	Distance to the closest wall of a point in the film [m]

Subscripts

$diff$	Diffusion
$evap$	Evaporation
f	Film
hf	Heat transfer fluid
i	Inlet
int	Interface
o	Outlet
sat	Saturation
tl	Triple line
v	Vapor
w	Wall

1 Introduction

For numerous years, a drastic increase in energy demand has been observed worldwide, mainly originating from fossil fuels, despite an alarming need for a decrease in energy consumption and CO_2 emission [1]. In the following years, the demand in cooling will further increase [2] and new solutions are needed to answer this need in an environmentally-friendly way. In this context, sorption systems look like a promising solution able to valorize waste energy at a low cost [3]. These systems also show the advantage of working with water, an abundant resource with zero global warming potential. The host of transfer in sorption machines are usually falling film exchanges, which are also used in a wide range of processes for their flexibility and high heat and mass transfer capacity. These exchanger are found in refrigeration [4, 5], heat pumps [6] or energy storage [7, 8] systems. Multiple technologies are considered for the exchanger of the machines, the two most dominant ones being horizontal tubes type or vertical plates types. The first category, where the fluid flows over horizontal tubes has been and still is thoroughly studied [9, 10, 11] and modelled [12, 13]. This geometry boast a high heat exchange capacity thanks to the easy addition of fins to the external surfaces [14]. However, a big downside of the horizontal tube system is their need for a high exchange surface [3]. To reduce the size of the machines, vertical plate falling film exchanger have seen a lot of interest in the recent years [15, 16] thanks to their low cost and high performance for a relatively small size.

Using water as the heat transfer medium has the heavy downside on needing to work at very low pressure (around 1 kPa). At this pressure, the systems' behaviour is drastically affected because of the very low vapor density which affects the bubble sizes and growth rates. Despite numerous advantages of the systems, there is a lack of scientific knowledge on the behaviour of the heat and mass transfer occurring during boiling processes at low pressure which lead to predominantly empirically designed system. To tackle this issue, a lot of effort have been made to improve the design and reduce the size of sorption systems. Most authors reported a very strong influence of the operating conditions on the performance of the machines [17, 18, 19, 20, 21]. Experimental studies also reported the appearance of complex phase-change mechanisms when condensing [17] water vapor or during boiling [22, 23] of the falling films in soprtion systems. Despite a very strong interest in understanding the inner workings of heat and mass transfer in falling liquid films by the community, either theoretically [24, 25, 26, 27] or experimentally [28, 29, 30, 31], the literature concerning the component scale of the sorption systems remains scarce and further knowledge on the behaviour of the flows inside of falling films exchanger is required.

Flat plate falling film evaporators an have important drawback in the form of a difficult distribution of the flow [32] and of important surface tension effects which often lead to the apparition of dry patches at the exchanger surface [33, 7], resulting in a drastic decrease in performance. To lift these limitations and increase the wetting of the exchanger plate, a lot of studies were undertaken on surface coating [34], texturing [35, 36, 37] or on the addition of surfactant [38, 39]. These studies showed a good improvement of the wetting of a flat vertical plate, however, none were able to guarantee a perfect wetting of the whole plate at all time. To circumvent this effect, Michel et al. [40] designed a grooved plate in order to insure a complete wetting of the exchange surface, even at very low flow rate. By sacrificing a part of the exchanger plate, the addition of fins between which the film flows enabled to create new contact lines ensuring that each flow never breaks. This study shown a significant improvement over a classic flat plate in the experiments but neglected to take account of the heat and mass transfer occurring in the vicinity of the triple contact line attached on the lateral fins.

In this study, a falling film grooved plate evaporator is studied. A pressure controlled enclosure has been designed to experimentally study the performance of the system. A numerical model has been developed to take account of the influence of the shape of the grooved plate on the heat and mass transfer of the component and has been compared to the experiments and a similar model considering a flat evaporator plate. The main goal of this study is to develop a simple yet effective heat and mass transfer model describing the behaviour of the evaporator plate taking account of the transfers at the triple contact line, with an added aim of being faster to compute than the one written in previous studies of the authors' group. After describing the experimental set-up, both models will be presented. Finally, the influence of the grooves on the heat and mass transfer will be discussed and the performance of the grooved evaporator will be studied.

2 Experimental set-up

Description of the system

The experimental set-up considered in the present paper is presented in Fig. 1. The liquid water is pumped from a temperature controlled tank to the distributor of the evaporator which distributes

the flow quite uniformly at the top of the vertical grooved plate. The liquid is then retrieved at the bottom of the plate by a funnel and returns to the initial tank. The falling film is heated by a heat transfer fluid (HTF) flowing in counter current mode in the exchanger. The temperature of the HTF is set by a thermostatic bath. This results in an increase of the water falling film temperature and to a partial evaporation of the liquid film. In order to control the pressure inside the enclosure at a fixed value of 10 mbar, a typical working pressure at the evaporator for water cooling system, a condenser made from a cooper spiral in which a cold sink heat transfer fluid flows is used. The temperature of the coolant is set so that water vapor condenses on the tube and flows down to a second funnel in order to return the initial tank. The flow of the falling film is characterized by the Reynolds number defined as:

$$Re = \frac{\Gamma}{\nu} \tag{1}$$

with Γ the volumetric flow rate per unit of width of wetted channel and ν the kinematic viscosity of the fluid.

The evaporator is made from two 3 mm thick and 250 mm long aluminium plates welded together. This assembly forms a plate heat exchanger with a filling film on one of its face. The HTF flows inside vertical channels with rectangular cross-sections placed face-to-face with the grooves of the falling film. The geometry of the evaporator plate is presented in Fig. 2. The water film flows down the 16 grooves 4 mm wide and 1 mm deep separated by 2 mm wide fins. The width of the grooves was chosen in a previous study to ensure the wetting of the entire base surface of the grooves [40]. This choice was made in the case of a desorber working with a water+LiBr solution where the capillary length of the solution is 2.25 mm in the working conditions. The width of the grooves ensures a good wetting of the surface at very low Reynolds numbers without trapping gas in the wedges, which would results in expelling the liquid from the groove due to surface tension forces. However, the higher wettability of the surface comes at the cost of dampening the surface perturbations, thus constraining the film flow to be almost flat. In the present case, pure water is studied. It's capillary length is 2.7 mm in working conditions, which is close to the value for water+LiBr mixture. It is considered that the design previously chosen by Michel et al. [40] is a suitable geometry adapted to the study of falling film evaporators, condenser, desorber and absober alike.

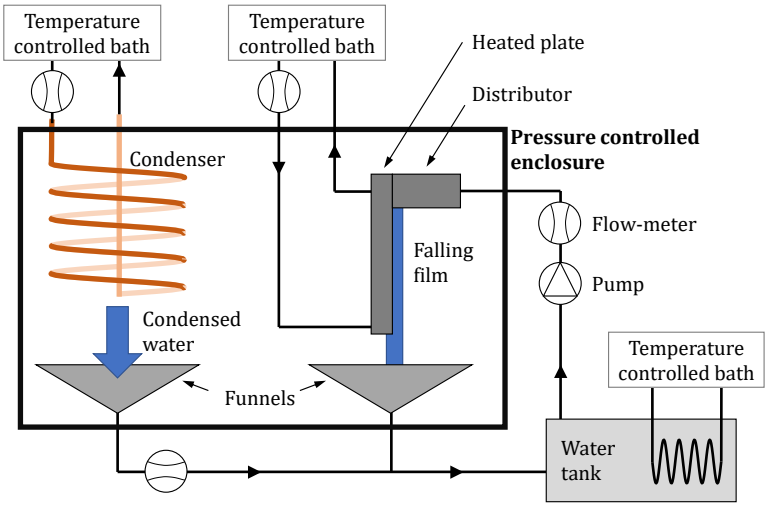

Figure 1: Scheme of the pressure-controlled falling film evaporator experimental set-up.

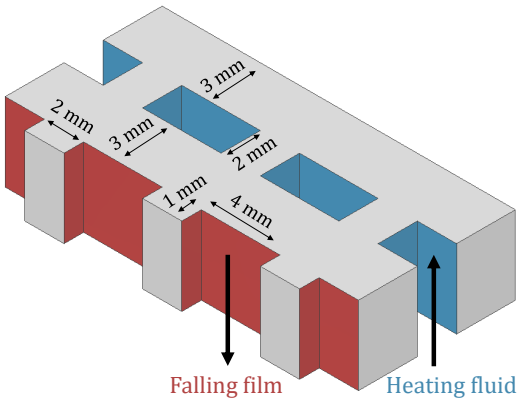

Figure 2: Cross-section view of the plate exchanger. The falling film flows down the free-surface grooves (in red) and the heating fluid counter-flow is located in the closed channels (in blue).

Measurement and uncertainties

The experimental setup is instrumented in order to characterize the vertical grooved evaporator plate performance. The pressure is measured by a ceramic pressure sensor (PFEIFFER VACCUM CMR 362) of accuracy ±0.2% of the measured value. The mass flow rate of each liquid line is monitored by Coriolis flow meters (MICRO-MOTION F025) of precision ±0.1%. Finally, PT-100 probes are used to record the liquid temperature at the inlet and outlet of each element of the set-up with a precision of ±0.1°C. The measurement were obtained at a frequency of 0.05 Hz integrated over 20 minutes periods (i.e. averaged over 60 points), reducing the random measurement error by a factor $\sqrt{60}$. A random draw Monte-Carlo method is used to evaluate the measurement error in the enthalpy balance of each flow based on the standard deviation of the output distribution. The error is estimated at ±1% for the film flow, ±3% for the HTF flow and ±4% for the condenser flow.

3 Heat and mass transfer models for liquid falling film evaporators

Flat film evaporator model

A 1D stationary model has been developed in previous studies to describe heat and mass transfer during water absorption and desorption on a vertical falling film in the context of vertical evaporators and desorbers. This model has already been described in details in previous papers [41, 33]. A simplified version is used for this study, thus only the main hypothesis and equations are presented thereafter. The evaporator model, presented in Fig. 3, is composed of a vertical wall surrounded on one side by the HTF and on the other side of the water falling liquid film, this side is placed in a saturated water vapor atmosphere. The length of the evaporator is discretized into small element of size dz. In each of the elements, the energy and mass balances of the system are solved under stationary conditions.

The following assumptions are made to solve the problem :

- The flow of the solution is laminar.
- The pressure in the vapor phase is considered homogeneous and constant. Moreover, it is supposed that no non-condensable gas (i.e. air) is present in the enclosure.
- The heat conduction in the wall in the flows direction is negligible.

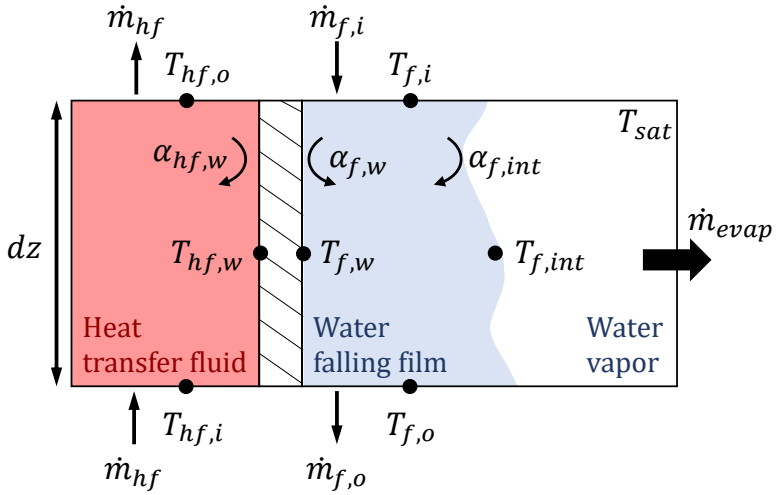

Figure 3: Diagram of a control element used in the resolution of the heat and mass transfer in the absorber/desorber model, simplified for pure water systems. The heating fluid (in red) is used to heat up and evaporate the water falling film (in blue) on the other side of the wall (striped box). Convective coefficients are used to evaluate the interactions between the different phases.

- The variations of kinetic and potential energies of the fluids are neglected.
- The heat and mass transfer equations are solved for the average temperature inside the element defined as $\overline{T} = \frac{T_o + T_i}{2}$.

From this set of assumptions, the mass and energy balances of the system are as follows :

Energy balance of the heat transfer fluid:

$$\dot{m}_{hf}\left(h_{hf,i} - h_{hf,o}\right) - \alpha_{hf,w}\, dz\, l\, \left(T_{hf,w} - \overline{T}_{hf}\right) = 0 \tag{2}$$

Energy balance at the HTF and wall interface:

$$\alpha_{hf,w}\, dz\, l\, \left(\overline{T}_{hf} - T_{hf,w}\right) + \frac{\lambda_w}{H_w}\, dz\, l\, \left(T_{hf,w} - T_{f,w}\right) = 0 \tag{3}$$

Energy balance at the falling film and wall interface:

$$\alpha_{f,w}\, dz\, l\, \left(\overline{T}_{f} - T_{hf,w}\right) + \frac{\lambda_w}{H_w}\, dz\, l\, \left(T_{hf,w} - T_{f,w}\right) = 0 \tag{4}$$

Mass and energy balance of the falling liquid film:

$$\dot{m}_{f,i} - \dot{m}_{f,o} + \dot{m}_{evap} = 0 \tag{5}$$

$$\dot{m}_{f,i}\, h_{f,i} - \dot{m}_{f,o}\, h_{f,o} + \dot{m}_{evap}\, h_{evap} + \alpha_{f,w}\, dz\, l\, \left(T_{f,w} - \overline{T}_{f}\right) = 0 \tag{6}$$

Energy balance at the liquid/vapor interface:

$$\dot{m}_{evap}\, h_{evap} - \alpha_{f,int}\, dz\, l\, \left(T_{f,int} - \overline{T}_{f}\right) = 0 \tag{7}$$

The convective heat transfer coefficients concerning the film $\alpha_{f,w}$ and $\alpha_{f,int}$ are calculated using correlations for laminar falling film flowing on a wall at constant temperature described in [42, 43]. In order to evaluate these coefficients, the thickness of the liquid film layer is required. The value is estimated using the equation defined in [44] for a laminar film considering a parabolic velocity profile.

The convective heat transfer coefficient between the HTF and the wall $\alpha_{hf,w}$ is calculated using the Dittus-Boelter equation for an internal flow when the flow is turbulent [45] and with the correlations described in [45, 12] when the flow is laminar. No transitional flow is considered in this model, the limit between laminar and turbulent regime is set at a fixed Reynolds number of 4000 (as defined in Eq. (1)).

Heat transfer at the fins and triple contact line evaporation for a perfectly flat film

The model described previously is written to be reversible, in order to be able to evaluate both absorption or desorption of water vapor by a liquid film. It showed a good prediction of water vapor absorption rate for a film Reynolds number under 150 [40] but was only validated for an absorber configuration. Furthermore, it does not accurately take account of the boundary effect introduced by the fins on the surface of the heat exchanger plate. The thickness of the film being 10 times smaller than it's width, the reduction of the heat and mass transfer close to the corner of the grooves was assumed to be compensated by the enlargement of the exchange surface. However, the fins increase the heat transfer due to the presence of triple contact lines. For pure fluids, the triple contact line appears to play a significant role in the case of evaporators, wheareas in the case of desorber, the effect is limited due to mass diffusion effects. This issue is really close to the ones encountered in heat pipes, where similar configurations have been studied [46, 47, 48]. In order to evaluate the influence of the fins, the heat and mass transfer in a 2D cross-section of the exchanger has been simulated in a steady state using a finite elements method. The modeled geometries are presented in Fig. 4, where the wall dimensions are the same as the one in the experiments. In each case, a single half-groove is considered. As a first approximation, the film is supposed to be be laminar and perfectly flat inside of the groove, this second assumption will be discussed later. Under these conditions, the velocity in the transverse direction of the flow is zero. The transfer in the fluid phase is thus considered to be purely diffusive. The vapor phase is considered saturated at a constant pressure of 10 mbar. At this pressure, it can be considered that the vapor molecular density is low enough in the vicinity of the evaporator to neglect the heat exchange between the vapor and the solid. The heat transfer at both lateral boundaries is zero due to the symmetries. At the liquid/vapor interface, a heat transfer coefficient α_{evap} is used to model the evaporation, the coefficient is obtained from the gas kinetic theory [44]:

$$\alpha_{evap} = \frac{2\,a}{2-a}\frac{\rho_v\,h_{evap}^2}{T_{sat}}\frac{1}{\sqrt{2\,\pi\,\frac{R}{M_v}\,T_{sat}}}\left(1-\frac{P_{sat}}{2\,\rho_v\,h_{evap}}\right) \tag{8}$$

where a is the accommodation coefficient, ρ_v the volumetric mass density of water vapor, T_{sat} the saturation temperature of the water vapor, R the ideal gas constant and M_v the molar mass of water vapor. This heat transfer coefficient is designed to take account of the particular evaporation physics at the triple contact line. Finally, a heat flux density is imposed at the bottom wall to simulate heat transfer from the HTF to the plate. The problem is solved using finite element method thanks to the Partial Differential Equation Toolbox of Matlab. The mesh was generated by imposing an element size of 10^{-8} m close the triple contact line and 10^{-6} m at the other interfaces. The elements were also allowed a regular growth of the size of the elements up to 10^{-6} m. The convergence criterion is set for a relative error between each step of 10^{-4}. Two exchanger plates geometry were considered, without (Fig. 4.a) and with (Fig. 4.b) a fin at the side of the liquid film, representing either a flat or a grooved exchanger plate. The heat flux density applied at the bottom wall. In order to quantify

the influence of the fins on the heat transfer, a heat transfer resistance is calculated. This resistance is used to evaluate the transfer from the HTF/wall interface to the vapor and is defined as:

$$R_{tl} = \frac{T_w - T_{sat}}{q_{calo}} \tag{9}$$

where q_{calo} is the total heat flux transmitted to the vapor and T_w is the temperature of the wall at the bottom interface. The transfer at the triple contact line is affected by the aspect ratio of the film. As a consequence, the thermal resistance R_{tl} is linked to the geometry of the exchanger plate and is integrated in the width of the groove.

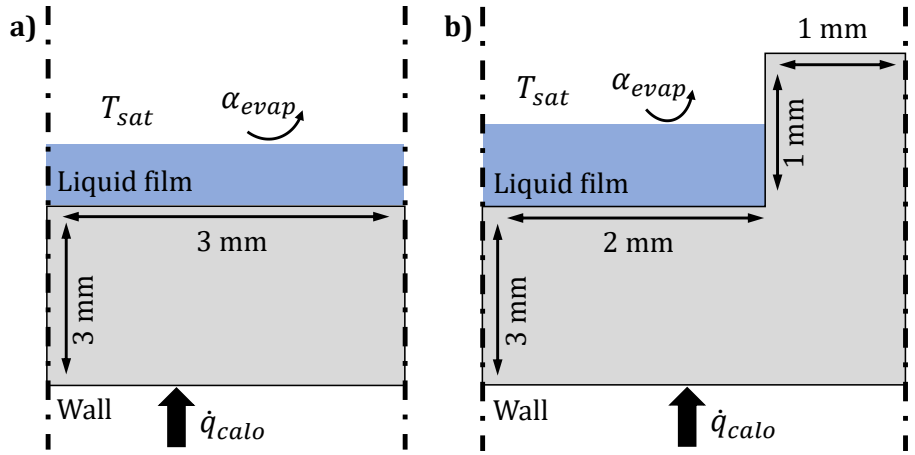

Figure 4: Cross-section schemes of flat film heat exchanger plates without (a) and with (b) fins. The film is slightly thicker in the second case because of the reduction of wetted surface area.

The Reynolds number of the film Re is a control parameter of the simulation. It can easily be linked to thickness of the film δ thanks to Eq. (1) and to the Nusselt flat film theory in the condition of a fully developed flow. The relation between the two quantities is expressed for a vertical film as:

$$\delta^3 = \frac{Re\, 3\, \nu^2}{g} \tag{10}$$

where g is the gravitational acceleration. The Nusselt flat film model is, however, not directly applicable to the grooved plate as the velocity field in the liquid phase is affected by the fins. The velocity field of the film flowing in a groove is calculated by constructing an approximate model derived from the Nusselt flat film solution, assuming the same set of hypothesis. The driving force of the flow is gravity, which is uniform in the flow direction. It is thus supposed that the growth rate of the velocity field is the same in both the x and y direction. Introducing d_w, the distance to the closest wall from any given point inside the liquid film, the velocity field in the liquid film flowing on a grooved plate is expressed as:

$$u(x, y) = \frac{g\, \delta^2}{2\, \nu} \left(\frac{2\, d_w}{\delta} - \frac{d_w}{\delta^2} \right) \tag{11}$$

From this definition, the flow rate and the Reynolds number are obtained for a given film thickness by integrating the velocity field of the liquid film. It is important to note that the Reynolds number for the grooved plate is slightly lower that for the flat plate for the same thickness of the liquid layer.

Nodal model for heat and mass transfer in falling film evaporator at the component scale

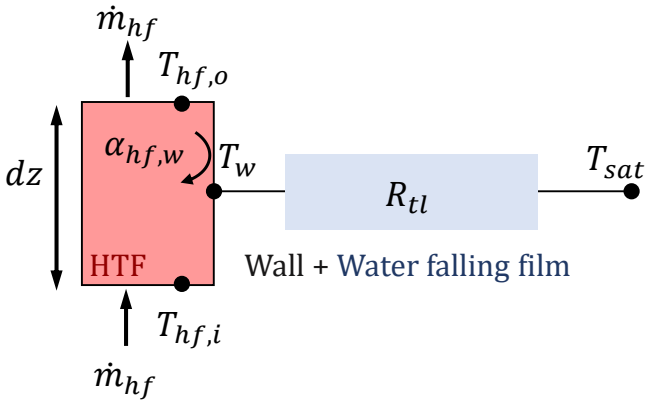

Figure 5: Heat and mass transfer model based on thermal resistances and energy balance at the heating fluid. The heat transfer through the fluid, including evaporation, is modelled by a thermal resistance R_{tl} obtained by simulation.

The simulations described previously are able to represent the heat transfer and to quantify the behaviour of the system for a wide range of working conditions thanks to the heat transfer resistance R_{tl}. This resistance accounts for the heat transfer from the wall/HRF interface to the vapor phase and can thus be used to replace this side of the transfers in the absorber/desorber model (Fig. 5).Based on this conclusion, nodal thermal model has been developed to evaluate the heat transfer and evaporation rate in the evaporator by taking account of the influence of the fins. Each groove of the evaporator are independently divided into multiple control volumes for which the energy balance equations are written, as is shown in Fig. 5. The transfer through the wall and the film are modelled by the thermal resistance R_{tl} obtained by simulation. The heat conduction in the wall in the flow direction is neglected. The governing equations of this model are:

Heat transfer and evaporation through the wall and the film:

$$\alpha_{hf,w}\, l\, dz\, \left(\overline{T}_{hf} - T_w\right) - \frac{T_w - T_{sat}}{R_{tl}}\, dz = 0 \tag{12}$$

Energy conservation at the HTF:

$$\dot{m}_{hf}\, Cp_{hf}\, \left(T_{hf,i} - T_{hf,o}\right) - \frac{T_w - T_{sat}}{R_{tl}}\, dz = 0 \tag{13}$$

The parameter $\alpha_{hf,w}$ is in common with the absorber/desorber model (Sec. 3) and is thus obtained by the same set of correlations [45, 12] and is evaluated at each node. The thermal resistance R_{tl} is evaluated only once for each film flow rate because the change in mass flow rate due to evaporation is considered negligible. The state of the heat exchanger is evaluated by exploring each nodes consecutively from the film inlet. The equilibrium state of the evaporator is solved by iterative process. At each iteration, the inlet temperature of the HTF is shifted by the difference between the expected value and the output value of the model until the temperature gradient in the HTF matches with it's imposed inlet temperature (at the film outlet). Knowing that the film flows in a saturated vapor atmosphere, the evaporation mass flow rate $\dot{m}_{evap}$ is obtained by integrating the heat flux transfered at each node:

$$\dot{m}_{evap}\, h_{evap} - \int_0^L \frac{T_w(z) - T_{sat}}{R_{tl}}\, dz = 0 \tag{14}$$

The bulk temperature of the film is obtained from the final solution of the heat transfer simulation at the outlet of the evaporator and is expressed as the mixing cup temperature:

$$\overline{T}_f(z) = \frac{\int_0^\delta \int_0^l T_f(x,y,z)\, u(x,y)\, dx\, dy}{\int_0^\delta \int_0^l u(x,y)\, dx\, dy} \tag{15}$$

The velocity field $u(x,y)$ considered depends on whether the evaporator plate is grooved or not, in the first case the Nusselt velocity profile is considered and in the grooved case, the velocity profile defined in Eq. (11) is used.

4 Results

Influence of the fins on the local heat transfer

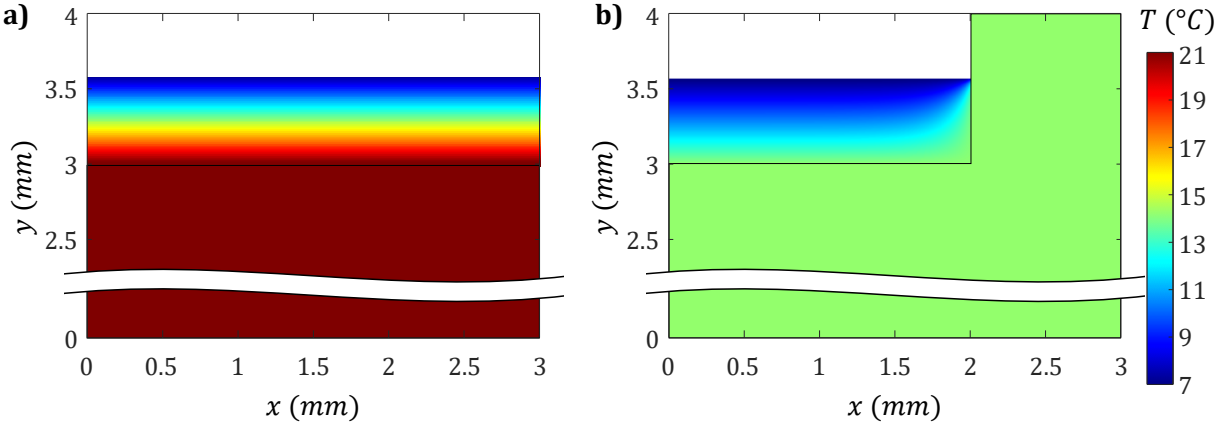

Figure 6: Fully developped temperature field results of the heat transfer simulation problem without (a) and with (b) grooves for a given flat film thickness $\delta = 0.6$ mm. These temperature fields are used to evaluate the heat transfer resistances through the plate and the film to the water vapor.

To evaluate the thermal resistances, the cross-section simulations in both cases were compared. A typical set of result is presented in Fig. 6, for a total heat flux at the bottom boundary of a half-groove of 18 W/m (value obtained from experiments). In this example, the thickness of the liquid layer is set at 0.6 mm for both films, which corresponds to a flow of Reynolds number $Re = 333$ for the film with no fins and $Re = 305$ for the one with the fins (based on the velocity obtained from Eq. (11)). In both cases, it can be observed that the temperature is quite uniform in the cross section of the wall and will be considered uniform in the following. As expected from the higher exchange surface, the equilibrium temperature of the wall is lower in the presence of fins at 14.21°C against 21.6°C for the flat wall surface. These different wall temperatures yields two different values of heat transfer resistance through the film, being respectively $R_{tl} = 0.43$ K m/W and $R_{tl} = 0.22$ K m/W for the cases without and with fins (as defined in Eq. (9)). A relative increase of the heat transfer of 50% is thus observed for a grooved plate compared to a flat plate at this given film thickness value.

The evolution of the heat transfer resistance with the thickness of the film has been evaluated, the results are presented on Fig. 7 and presented for a range of Reynolds number from 12 to 787. This values correspond to typical working ranges of falling film exchanger where the thickness of the film varies from 0.2 to 0.8 mm. It can be observed that the intensification of the heat transfer due to the

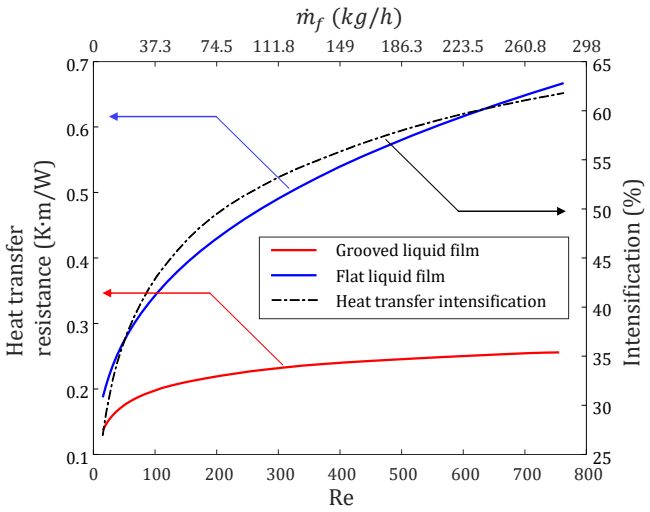

Figure 7: Heat transfer resistance through a flat liquid film flowing either on a grooved exchanger plate (red) or on a perfectly flat surface (blue). The black dotted line is the intensification due to the heat transfer enabled by the fins, evaluated relative to the perfectly flat surface.

fins increases when the thickness of the film increases. This is expected because the exchange surface with the fins increase linearly with the thickness δ of the film, because the transfer at the triple contact line is unaffected by the change in thickness and because the diffusive transfer from the bottom of the groove decreases linearly with δ^2. In the working range of the exchanger, an increase of heat transfer ranging from 25% to 60% can be expected when grooving the plate.

In the range studied in Fig. 7, it is observed that the rate of change of the heat transfer resistance for the grooved exchanger decreases with the increase of the Reynolds number grows higher. At this point, it is unsure if an asymptotic value exists or if the thermal resistance will continue to grow infinitely. To answer this question, the evolution of the heat transfer resistance through a grooved film has been studied until the thickness of the film becomes the same as the width of the half-groove (i.e. for $\delta \leq 2$ mm). This value is the limit after which any point of the free surface is closer to the fin than to the bottom of the groove, diffusion in the horizontal direction then becomes more influential than in the vertical direction. The result of this study is presented in Fig. 8 where the heat transfer resistance for a grooved film (in red) is compared to the resistance for a film where the bottom of the groove has been isolated (in blue). This second case considers only the transfer from the fin to the vapor through the liquid film, meaning that diffusion is considered only in the x direction. Thus, this configuration represents only the part of the heat transfer introduced by the fins. It appears that this case attains a minimum asymptotic value for the heat transfer resistance of $R = 0.32$ K m/W, which is the maximum value that can be reached by a film flowing in a groove, as diffusion in the vertical direction always plays a role in the transfer. This asymptotic value is attained in the case of the flat film flowing on the flat plate for $Re = 80$ in Fig. 7 (i.e. $\delta = 0.375$ mm). In a majority of configuration, it is quite impossible to maintain whole surface wetting at such a low Reynolds number [33] and rivulets tends to form downflow. Furthermore, the heat transfer increase due to the fins compares well with the increase induced by perturbatives waves at the surface of the film of around 30% [28, 49, 50], that is lost when constraining the flow in grooves. As a consequence, for the same effective exchange surface area of the exchanger plate, the heat transfer with grooves and without surface waves is of roughly

the same magnitude as a configuration without groove in the presence of surface waves (considering perfect wetting). Thus, grooved plates seem like a very good solution for vertical plates exchangers as the wetted area is always maximized and heat transfer at the fins increases the efficiency of the system. Moreover, the transfer at the triple contact line enables a minimum evaporation rate for any film flow rate.

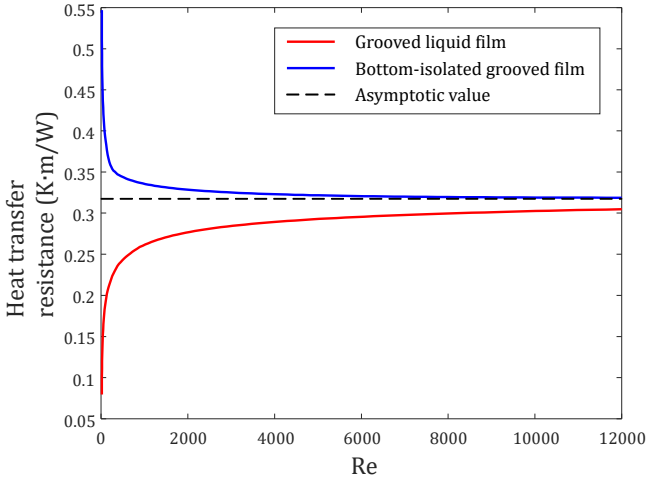

Figure 8: Heat transfer resistance through a flat liquid film flowing on a grooved exchanger plate. The blue line is obtained in the case of a liquid film isolated at the bottom of the groove, enabling the determination of an asymptotic value for the transfer at the side and triple contact line of the film.

Influence of the curvature of the free surface of the film

Until this point, only perfectly flat films were considered. However, the free surface of the liquid layer is curved inside of the grooves due to the surface tension forces. In order to better represent the evaporator, the curvature of the film surface has been introduced in the model. The shape of the free surface has been experimentally measured on the evaporator plate at ambient pressure using a CCI probe (STIL Optics CCS Prima). Because the plate is not accessible when the pressure controlled enclosure is closed, it is supposed that the free surface curvature is not affected by the pressure in the vapor phase (i.e. the falling film hydrodynamic is not affected by the pressure and remains unchanged). The curvature of the free surface of the film has been characterized for three values of the Reynolds number : 70, 140 and 210, in decreasing order. The three measured curvature are presented in Fig. 9. It can be observed that the wetting of the fin decreases very little when diminishing the flow rate and the contact line seems to have stuck to the top of the fin. It is possible that the surface tension force is sufficiently high so that any wetted part of the film remains wetted when decreasing the flow rate. This can however, hardly be taken account of in the simulation as the adherence of the film to the wall is a consequence of a hysteresis effect that would require further investigation. Moreover, the equilibrium shape attained in the evaporator is yet unknown, the hysteresis effect might not exist when the film is heated: as the pressure inside the enclosure is constant, the curvature of the film may be constant. Because the triple contact line is a privileged evaporation area, it can be expected to recede if the flow rate is not sufficiently high to maintain the layer in the almost-null velocity zone. It is thus quite difficult to devise a method to numerically evaluate the curvature of the free surface at a given flow rate without further knowledge.

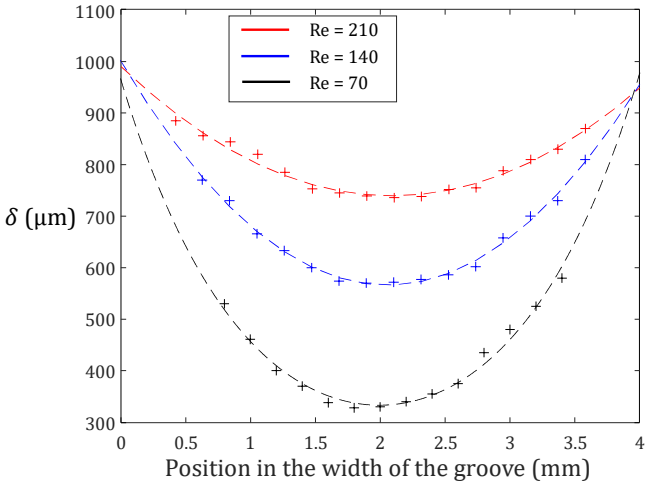

Figure 9: Curvature of the free surface of the falling film inside a groove measured using a CCI probe for three Reynolds number values 70, 140 and 210. The measurement where taken in decreasing order, with the aim of maximizing the wetted surface. The measured curvatures (cross) were fitted (dotted lines) using a quadratic polynomial.

The influence of the curvature of the free surface has been studied by introducing the shape of the liquid layer in the heat transfer simulation, the results are presented in Fig. 10. In this figure, Reynolds number has been calculated by approximating the velocity field of the liquid calculated from Eq. 11, based on the average thickness of the film. It is observed that the heat transfer resistance is lower with the higher curvature of the free surface, which was expected due to the reduction of the thickness liquid layer far from the fin (i.e. at the center of the channel) which increases the temperature gradient in this direction. However, the value of heat transfer resistance is little affected by the curvature. In Fig. 10.b, the relative difference of the curved resistance compared to the flat film is plotted. For $Re > 100$, the difference is very little, under 5%. For $Re < 100$, a significant difference is only observed for the two higher curvature, attaining a maximum of 12% for $Re = 40$ under which dewetting occurred at the center of the channel. However, it is very difficult to ponder whether these flows are representative of reality as a liquid film thickness under 100 μm at the middle of the film is very likely to break due to surface tension forces. It is also observed that the heat transfer resistance for the intermediate curvature case travels from the high curvature curve at low Reynolds number to the low curvature curve at high Reynolds number with a slight shift compared to the experimentally measured shapes. This effect denotes the transition where the improvement due to the decrease in diffusion length at the center of the channel becomes negligible compared to the global heat transfer, suggesting that the thinning of the free surface holds almost no effect for $Re > 200$. Given the complexity of assigning a film shape to a flow rate without considering a anterior state and despite an improvement in heat transfer resistance at low Reynolds number, the curvature can reasonably be neglected.

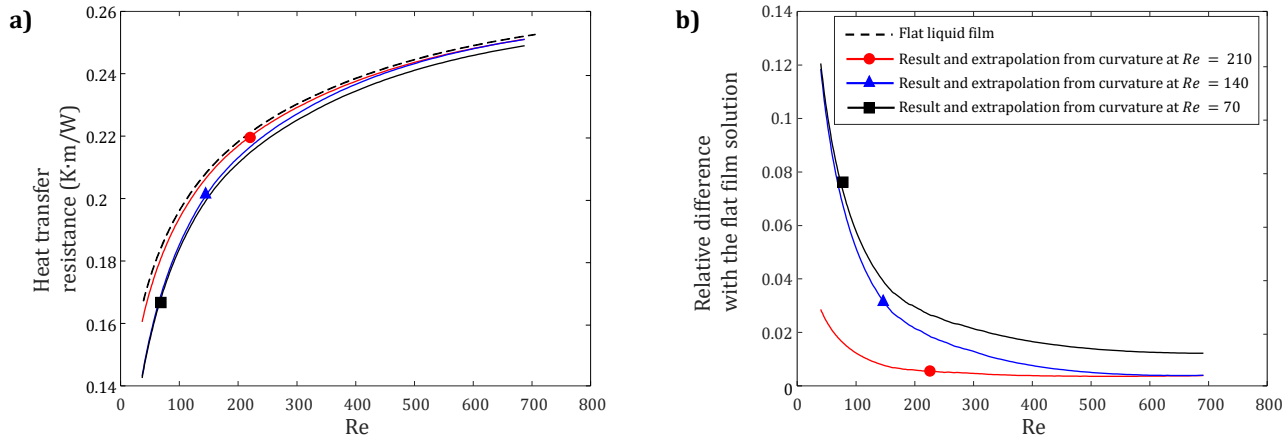

Figure 10: Influence of the curvature of the free surface of the film on the heat transfer coefficient. The three considered free surface shapes are based on the experimental results presented in Fig 9, the curvatures were extrapolated to a large Reynolds number range in order to draw a envelope of the impact on heat transfer. a) represents the heat transfer resistance values calculated for the four curvature configuration and b) evaluates the relative differences of the heat transfer resistances for the curved interface compared to the flat film solution.

Validation of the models against experimental measurements at component scale

The two exchanger models have been compared to experimental results obtained for a set of working conditions: two Reynolds numbers values for both the film and the HTF. In Fig. 11, the results are presented in the form of a relative difference between the models and the experiments compared to the experimental value as a function of the overheating of the HTF compared to the saturation temperature of the liquid film. It appears that both models underestimates the evaporation rate for an overheating temperature under 6°C, by around 10% for the present model compared to around 30% for michel et al. model. Above 6°C of overheating, the present model starts to overestimate the evaporation rate by around 5% while the model developed by michel et al. still the value by around 15%. This sudden change in the relative difference value can be explained by the presence of noncondensable gases in the water tank which starts to form bubbles in the film and thus reduces the heat transfer from the wall to the liquid.

It is observed that the difference between both models remains stable for the complete set of conditions. In the presented cases, both models are outputting very similar cooling for the HTF, with an underestimation of the decrease in temperature of the fluid between the input and the output of the plate by an error under 10%. The models differ, however, in the proportion of the energy distributed to the latent heat of vaporization or to the specific heat used to overheat the liquid film. The input/output temperature difference of the liquid film is very well estimated for the evaporator model, with an underestimation error lower than 2%, while michel et al.'s model globally overestimates it by an error of 100%. This shows that taking account of the presence of the grooves is crucial in sizing a plate exchanger. This is mainly due to the important effect of the fins on the heat transfer to the film and especially because they introduce a triple contact line where phase change is highly promoted.

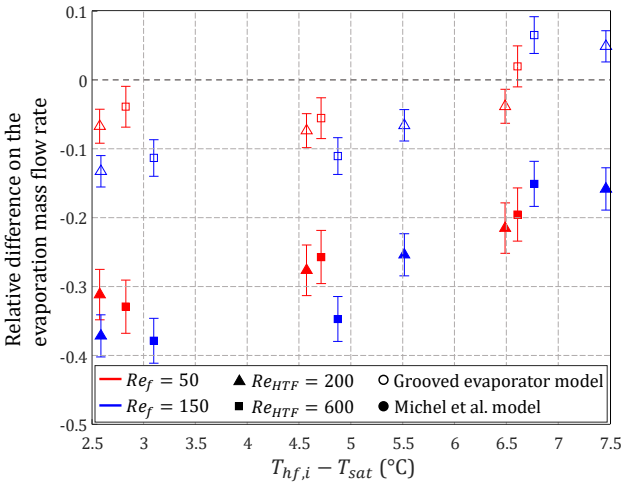

Figure 11: Relative difference on the evaporated mass flow rate between the experimental data and the results obtained from the grooved evaporator model (hollow symbols) and from Michel et al. model (full symbols). The comparison are presented for two film Reynolds number 50 (red) and 150 (blue) and two HTF Reynolds number 200 (triangles) and 600 (squares).

Efficiency of the evaporator

Thanks to the previous results, the performance of a grooved plate evaporator can be estimated for a wide span of working conditions. The efficiency ε is defined as the ratio between the retrieved and the retrievable heat at the HTF :

$$\varepsilon = \frac{T_{calo,i} - T_{calo,o}}{T_{calo,i} - T_{sat}} \tag{16}$$

where the indexes i and o denote the inlet and the outlet of the plate. The model assumes the flow to be fully thermally developed everywhere on the plate. The establishment length L_{th} of the thermal boundary layer in the falling film can be expressed for a flat film as [40] :

$$L_{th} = \frac{17}{640}\,\delta\, Re\, Pr \tag{17}$$

where Pr is the Prandtl number of the liquid. At Re = 300, the thermal establishment length is $L_{th} = 29.6$ mm, which is still small compared to the full plate length of $L = 250$ mm. Thus it can be considered that the model is able to correctly estimate behaviour of the evaporator for falling film Reynolds number under 300. The efficiency of the evaporator is calculated for a Reynolds range of 3-300 for the liquid film and 45 to 700 for the HTF. It is important to note that, given the formulation of the model, the results of the calculation are purely linear with the HTF inlet temperature. Thus, the value of the overheating does not impact the estimated effectiveness of the evaporator. The efficiency map of the evaporator obtained thanks to the model presented in this paper is presented in Fig. 12. Fig. 12.a shows that the efficiency is, as expected, maximum for the couple of lowest Reynolds numbers at a maximum of 99%. Moreover, the Reynolds number of the liquid film matters very little in the studied range and is only affecting significantly the efficiency in the 3 to 50 range, which is in good agreement to the observation made on Fig. 7. However, The Reynolds number of the HTF influences greatly the efficiency with a very sharp decrease from 88% at $\mathrm{Re_{HTF}} \simeq 75$ to 53% at $\mathrm{Re_{HTF}} \simeq 200$. This map is to be compared to the one presented in Fig. 12.b where the heat flux density $\dot{q}$ taken at

the HTF injected at an overheat temperature $T_{HTF,i} - T_{sat} = 5°C$, given the surface of the evaporator plate. It is important to note that, as the model is based on temperature gradients alone and assume a fully developed regime in the film side, the efficiency map (Fig. 12.a) is unaffected by the overheat temperature and thus that the heat flux absorbed at the HTF (Fig. 12.b) varies linearly with the overheat temperature. The second map highlights that, despite the efficiency being the highest at low Reynolds number, the heat flux density is quite low in this regime. The better working condition appear to be a high Reynolds number for the HTF and the lowest Reynolds number achievable for the falling film which would maximize the evaporation mass flow rate.

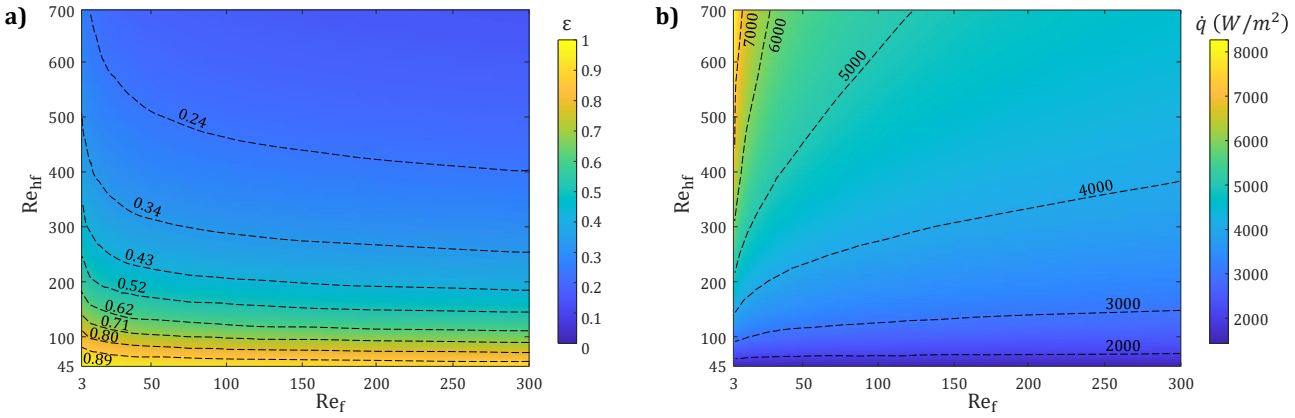

Figure 12: Maps of the operating regimes of the evaporator. a) represents the efficiency ε of the grooved evaporator as a function of the liquid film and of the HTF Reynolds number and b) represents the heat flux density $\dot{q}$ extracted at the HTF for an inlet overheat temperature of 5°C. The dotted curves are isolines of the specified efficiency value.

5 Conclusion

This study investigates a flat falling film evaporator heated by a HTF at counter-current flow configuration. The exchanger plate is grooved in order to avoid de-wetting of the surface and increase the effective exchange surface. A side effect of the grooved plate is the introduction of fins which influences the heat and mass transfer through the film. The quantification of the evaporation capacity of the system is key in its sizing. Modelling and experiments were confronted to quantify the generated vapor rate and the capacity of the evaporator to extract heat from the HTF. The experiments were carried on a pressure-controlled test bench designed to evaluate the performance of evaporator plates in stationary conditions. This study investigated a specific plate 250 mm long and 100 mm wide (discretized in 16 grooves 4 mm wide separated by 2 mm fins). The bench allows to evaluate a wide range of operating conditions (pressure, flow rates, temperatures).

To quantify the effect of the fins on the heat and mass transfers, a 2D stationary simulation in the cross-section of the exchanger has been developed. The results highlighted the tremendous importance of the triple contact line between the liquid film, the fin and the water vapor. In particular, the grooved geometry allows for an increase in heat transfer of around 30 to 50% compared to a perfectly flat film without grooves at the same Reynolds number. This increase is of the same order of magnitude as the one induced by surface waves that appear for films flowing on perfectly flat plates. Thus, the presence

of grooves in the exchanger plate is a excellent answer to solve the wetting difficulties in falling film evaporators without any significant downside.

A 1D model has been developed based on the aforementioned simulations to describe the heat transfer from the HTF to the liquid film and to quantify the water evaporation rate over the complete evaporator plate exchanger. This model has been compared to a previously developed model not taking account of the presence of fins and both were confronted against experimental results. It was highlighted that the model developed in this paper shown a better estimation of the operating conditions of the evaporator while being much simpler. The effectiveness of the exchanger and the heat flux density extracted at the HTF for a wide range of both fluid flow rates and optimal working range were highlighted.

To increase the performance of the grooved evaporator plate, the main option is to decrease the depth of the HTF flow channels which would increase the channel volume to exchange surface ratio and would enable the thermal boundary layer to grow closer to the center of the channel. Further studies on the test bench would enable a better understanding of the phase change phenomenon taking place in vertical falling film.

Acknowledgments

The authors acknowledge support by the FRAISE project, grant ANR-16-CE06-0011 of the French National Research Agency (ANR).

The authors would like to thank Florine Giraud who made the measurements of the film thickness and provided the results and who generally was a great help by sharing her insights on the subject.

References

[1] IPCC. Impacts, adaptation and vulnerability - summary for policymakers, 2022.

[2] IEA. The future of cooling - opportunities for energy-efficient air conditioning, 2018.

[3] Amín Altamirano, Benoit Stutz, and Nolwenn Le Pierrès. Review of small-capacity single-stage continuous absorption systems operating on binary working fluids for cooling: Compact exchanger technologies. *International Journal of Refrigeration*, 114:118–147, 2020.

[4] A. Aliane, S. Abboudi, C. Seladji, and B. Guendouz. An illustrated review on solar absorption cooling experimental studies. *Renewable and Sustainable Energy Reviews*, 65:443–458, 2016.

[5] A. Altamirano, N. Le Pierrès, B. Stutz, and A. Coronas. Performance characterization methods for absorption chillers applied to an nh3-lino3 single-stage prototype. *Applied Thermal Engineering*, 185:116435, 2021.

[6] Jing Zhang, Hong-Hu Zhang, Ya-Ling He, and Wen-Quan Tao. A comprehensive review on advances and applications of industrial heat pumps based on the practices in china. *Applied Energy*, 178:800–825, 2016.

[7] K. Edem N'Tsoukpoe, Hui Liu, Nolwenn Le Pierrès, and Lingai Luo. A review on long-term sorption solar energy storage. *Renewable and Sustainable Energy Reviews*, 13(9):2385–2396, 2009.

[8] Devrim Aydin, Sean P. Casey, and Saffa Riffat. The latest advancements on thermochemical heat storage systems. *Renewable and Sustainable Energy Reviews*, 41:356–367, 2015.

[9] J. Killion and S. Garimella. Gravity-driven flow of liquid films and droplets in horizontal tube banks. *International Journal of Refrigeration*, 26(5):516–526, 2003.

[10] J.I. Yoon, T.T. Phan, C.G. Moon, H. Lee, and S. Jeong. Heat and mass transfer characteristics of a horizontal tube falling film absorber with small diameter tubes. *Heat and Mass Transfer*, 44(4):437–444, Feb 2008.

[11] S. Lee, L.K. Bohra, S. Garimella, and A.K. Nagavarapu. Measurement of absorption rates in horizontal-tube falling-film ammonia-water absorbers. *International Journal of Refrigeration*, 35(3):613–632, 2012. Refrigeration and Heat Pumping with Sorption Processes.

[12] J. D. Killion and S. Garimella. A critical review of models of coupled heat and mass transfer in falling-film absorption. *International Journal of Refrigeration*, 24(8):755 – 797, 2001.

[13] C. Zhao, D. Qi, W. Ji, P. Jin, and W. Tao. A comprehensive review on computational studies of falling film hydrodynamics and heat transfer on the horizontal tube and tube bundle. *Applied Thermal Engineering*, 202:117869, 2022.

[14] R. Volmer, J. Eckert, G. Füldner, and L. Schnabel. Evaporator development for adsorption heat transformation devices – influencing factors on non-stationary evaporation with tube-fin heat exchangers at sub-atmospheric pressure. *Renewable Energy*, 110:141–153, 2017.

[15] D. Sterner and B. Sunden. Performance of plate heat exchangers for evaporation of ammonia. *Heat Transfer Engineering*, 27(5):45–55, 2006.

[16] A. Gonda, P. Lancereau, P. Bandelier, L. Luo, Y. Fan, and S. Benezech. Water falling film evaporation on a corrugated plate. *International Journal of Thermal Sciences*, 81:29–37, 2014.

[17] S. Ben Jabrallah, A. Belghith, and J.P. Corriou. Convective heat and mass transfer with evaporation of a falling film in a cavity. *International Journal of Thermal Sciences*, 45(1):16–28, 2006.

[18] S.W. Chang, D.C. Lo, K.F. Chiang, and C.Y. Lin. Sub-atmospheric boiling heat transfer and thermal performance of two-phase loop thermosyphon. *Experimental Thermal and Fluid Science*, 39:134–147, 2012.

[19] H. Chen and R.S. Jebson. Factors affecting heat transfer in falling film evaporators. *Food and Bioproducts Processing*, 75(2):111–116, 1997.

[20] P.C. Thimmaiah, A. Sharafian, M. Rouhani, W. Huttema, and M. Bahrami. Evaluation of low-pressure flooded evaporator performance for adsorption chillers. *Energy*, 122:144–158, 2017.

[21] Z.Z. Xia, G.Z. Yang, and R.Z. Wang. Experimental investigation of capillary-assisted evaporation on the outside surface of horizontal tubes. *International Journal of Heat and Mass Transfer*, 51(15):4047–4054, 2008.

[22] F. Giraud, C. Toublanc, R. Rullière, J. Bonjour, and M. Clausse. Experimental study of water vaporization occurring inside a channel of a smooth plate-type heat exchanger at subatmospheric pressure. *Applied Thermal Engineering*, 106:180–191, 2016.

[23] F. Giraud, P. Vallon, and B. Tremeac. Experimental study of water vaporization occurring inside the channel of a smooth-plate type heat exchanger connected to an adsorber and comparison with trends observed in absorption configuration. *International Journal of Refrigeration*, 77:60–74, 2017.

[24] N. Cellier and C. Ruyer-Quil. A new family of reduced models for non-isothermal falling films. *International Journal of Heat and Mass Transfer*, 154:119700, 2020.

[25] A.N. Chernyavskiy and A.N. Pavlenko. Numerical simulation of heat transfer and determination of critical heat fluxes at nonsteady heat generation in falling wavy liquid films. *International Journal of Heat and Mass Transfer*, 105:648–654, 2017.

[26] G.F. Dietze. Effect of wall corrugations on scalar transfer to a wavy falling liquid film. *Journal of Fluid Mechanics*, 859:1098–1128, 2019.

[27] A. Miyara. Numerical analysis on flow dynamics and heat transfer of falling liquid films with interfacial waves. *Heat and Mass Transfer*, 35(4):298–306, 1999.

[28] R. Collignon, O. Caballina, F. Lemoine, and G. Castanet. Temperature distribution in the cross section of wavy and falling thin liquid films. *Experiments in Fluids*, 62(5):115, 2021.

[29] R. Collignon, O. Caballina, F. Lemoine, and G. Castanet. Simultaneous temperature and thickness measurements of falling liquid films by laser-induced fluorescence. *Experiments in Fluids*, 63(4):68, 2022.

[30] R. Mathie, H. Nakamura, and C.N. Markides. Heat transfer augmentation in unsteady conjugate thermal systems – part ii: Applications. *International Journal of Heat and Mass Transfer*, 56(1):819 – 833, 2013.

[31] A. Schagen and M. Modigell. Local film thickness and temperature distribution measurement in wavy liquid films with a laser-induced luminescence technique. *Experiments in Fluids*, 43(2):209–221, 2007.

[32] M.S. El-Genk and H.H. Saber. An Investigation of the Breakup of an Evaporating Liquid Film, Falling Down a Vertical, Uniformly Heated Wall . *Journal of Heat Transfer*, 124(1):39–50, 2001.

[33] F. Huaylla, B. Stutz, and N. Le Pierrès. Numerical and experimental analysis of falling-film exchangers used in a libr–h2o interseasonal heat storage system. *Heat Transfer Engineering*, 40(11):879–895, 2019.

[34] J. Wei, X. Xu, J. Zhang, and J. Liu. Measurement of liquid film coverage on vertical plates with hydrophilic and structured surface treatments. *Industrial & Engineering Chemistry Research*, 60(9):3736–3744, 2021.

[35] R. Chen, M. Lu, V. Srinivasan, Z. Wang, H. Cho, and A. Majumdar. Nanowires for enhanced boiling heat transfer. *Nano Letters*, 9(2):548–553, 2009.

[36] J. Lu, Z. Liu, W Xu, and J. Liu. Experimental study of the falling film evaporative cooling on horizontal tubes plates. *International Journal of Refrigeration*, 138:108–117, 2022.

[37] J. Wei, J. Liu, X. Xu, and X. Lu. Experimental and theoretical analysis of water spreading on horizontal grooved surfaces. *Chemical Engineering Science*, 249:117304, 2022.

[38] B. Y. Rubinstein and S. G. Bankoff. Dynamics of thin liquid films on a coated solid surface with insoluble surfactants: Weakly nonlinear analysis. *Langmuir*, 17(4):1306–1307, 2001.

[39] D.S. Kim and C.A. Infante Ferreira. Flow patterns and heat and mass transfer coefficients of low reynolds number falling film flows on vertical plates: Effects of a wire screen and an additive. *International Journal of Refrigeration*, 32(1):138–149, 2009.

[40] B. Michel, N. Le Pierrès, and B. Stutz. Performances of grooved plates falling film absorber. *Energy*, 138:103–117, 2017.

[41] F Huaylla, N Le Pierrès, B Stutz, and Edem N'Tsoukpoe. Performance analysis of multifunctional exchangers implemented in an interseasonal sorption heat storage system. In *ISHPC (International Sorption Heat Pump Conference), Maryland (USA)*, 2014.

[42] N. Brauner. Non-isothermal vapour absorption into falling film. *International Journal of Heat and Mass Transfer*, 34(3):767–784, 1991.

[43] G. Grossman. Simultaneous heat and mass transfer in film absorption under laminar flow. *International Journal of Heat and Mass Transfer*, 26(3):357–371, 1983.

[44] V.P. Carey. *Liquid-Vapor Phase-Change Phenomena: An Introduction to the Thermophysics of Vaporization and Condensation Processes in Heat Transfer Equipment.* CRC Press, 3rd edition, 2020.

[45] Frank P Incropera, David P DeWitt, Theodore L Bergman, Adrienne S Lavine, et al. *Fundamentals of heat and mass transfer*, volume 6. Wiley New York, 1996.

[46] R. Bertossi, Z. Lataoui, V. Ayel, C. Romestant, and Y. Bertin. Modeling of thin liquid film in grooved heat pipes. *Numerical Heat Transfer, Part A: Applications*, 55(12):1075–1095, 2009.

[47] V. S. Jasvanth, , A. Amritand, A.A. Abhijit, and J.H. Arakeri. Numerical investigation of an evaporating meniscus in a heated capillary slot. *Heat and Mass Transfer*, 55(12):3675–3688, Dec 2019.

[48] F. Lefèvre, R. Rullière, G. Pandraud, and M. Lallemand. Prediction of the temperature field in flat plate heat pipes with micro-grooves – experimental validation. *International Journal of Heat and Mass Transfer*, 51(15):4083–4094, 2008.

[49] David P Frisk and E.James Davis. The enhancement of heat transfer by waves in stratified gas-liquid flow. *International Journal of Heat and Mass Transfer*, 15(8):1537 – 1552, 1972.

[50] P.N. Yoshimura, T. Nosoko, and T. Nagata. Enhancement of mass transfer into a falling laminar liquid film by two-dimensional surface waves—some experimental observations and modeling. *Chemical Engineering Science*, 51(8):1231–1240, 1996.